AD-A277 583

(12)

ARL-TR-93-15

Copy No. 67

Bottom Backscatter from Trapped Bubbles

Final Report under Contract N00039-91-C-0082,
TD No. 01A1029, Bottom Backscatter from Trapped Bubbles

Frank A. Boyle
Nicholas P. Chotiros

Applied Research Laboratories
The University of Texas at Austin
P. O. Box 8029 Austin, TX 78713-8029

30 July 1993

Final Report

23 December 1991 - 31 December 1992

Destruction Notice: - For classified documents, follow the procedures in
DoD Manual 5200.22-M, Industrial Security Manual.
For unclassified, limited distribution documents, destroy by any method
that will prevent disclosure of contents or reconstruction of the document.

4176

94-09733

Approved for public release; distribution is unlimited.

DTIC
ELECTE
MAR 31 1994
S E D

Prepared for:
Naval Research Laboratory
Stennis Space Center, MS 39529-5004

Monitored by:
Space and Naval Warfare Systems Command
Department of the Navy
Washington, DC 20363-5100

94 3 31 034

REPORT DOCUMENTATION PAGE

Form Approved
OMB No. 0704-0188

Public reporting burden for this collection of information is estimated to average 1 hour per response, including the time for reviewing instructions, searching existing data sources, gathering and maintaining the data needed, and completing and reviewing the collection of information. Send comments regarding this burden estimate or any other aspect of this collection of information, including suggestions for reducing this burden, to Washington Headquarters Services, Directorate for information Operations and Reports, 1215 Jefferson Davis Highway, Suite 1204, Arlington, VA 22202-4302, and to the Office of Management and Budget, Paperwork Reduction Project (0704-0188), Washington, DC 20503.

1. AGENCY USE ONLY (Leave blank)	2. REPORT DATE	3. REPORT TYPE AND DATES COVERED
	30 Jul 93	final, 23 Dec 91 - 31 Dec 92

4. TITLE AND SUBTITLE
Bottom Backscatter from Trapped Bubbles, Final Report under Contract N00039-91-C-0082, TD No. 01A1029, Bottom Backscatter from Trapped Bubbles

5. FUNDING NUMBERS
N00039-91-C-0082,
TD No. 01A1029

6. AUTHOR(S)
Boyle, Frank A. Chotiros, Nicholas P.

7. PERFORMING ORGANIZATION NAMES(S) AND ADDRESS(ES)
Applied Research Laboratories
The University of Texas at Austin
P.O. Box 8029
Austin, Texas 78713-8029

8. PERFORMING ORGANIZATION REPORT NUMBER
ARL-TR-93-15

9. SPONSORING/MONITORING AGENCY NAME(S) AND ADDRESS(ES)
Naval Research Laboratory
Stennis Space Center, Mississippi 39529-5004

Space and Naval Warfare Systems Command
Department of the Navy
Washington, D.C. 20363-5100

10. SPONSORING/MONITORING AGENCY REPORT NUMBER

11. SUPPLEMENTARY NOTES

12a. DISTRIBUTION/AVAILABILITY STATEMENT
Approved for public release; distribution is unlimited.

12b. DISTRIBUTION CODE

13. ABSTRACT (Maximum 200 words)

A model for acoustic backscatter from gas bubbles in sediment has been developed. It computes the backscattering strength of a gassy sediment, given a spherical source in the water column above. A Biot model for acoustic penetration into the sediment is incorporated. The computed backscattering strength is that of a spatial distribution of trapped bubbles The bubble size distribution is assumed to mirror the pore size distribution. An approximate pore size distribution is estimated from the measured grain size distribution and studies of dense random packings of hard spheres.

14. SUBJECT TERMS
backscatter, bubble size distribution, pore pressure, reciprocity, Biot, gassy sediment, porous medium, sediment, bubble, plane wave decomposition, scattering cross section

15. NUMBER OF PAGES
49

16. PRICE CODE

17. SECURITY CLASSIFICATION OF REPORT	18. SECURITY CLASSIFICATION OF THIS PAGE	19. SECURITY CLASSIFICATION OF ABSTRACT	20. LIMITATION OF ABSTRACT
UNCLASSIFIED	UNCLASSIFIED	UNCLASSIFIED	SAR

This page intentionally left blank.

TABLE OF CONTENTS

Accesion For
NTIS CRA&I ☒
DTIC TAB ☐
Unannounced ☐
Justification .....
By .....
Distribution /
Availability Codes
Dist | Avail and / or Special
A-1

This page intentionally left blank.

LIST OF FIGURES

This page intentionally left blank.

PREFACE

This report is the final report of work that ARL:UT was tasked to perform under Contract N00039-91-C-0082, TD No. 01A1029, entitled Bottom Backscatter from Trapped Bubbles.

This page intentionally left blank.

1. INTRODUCTION

The objective of this work is an improved model for high frequency acoustic backscatter from shallow water sediment at shallow grazing angles. Initial development of a model was accomplished by Boyle and Chotiros in 1992 (ARL-TR-92-12).[1] This work included studies of a Biot model for acoustic transmission and reflection, originally developed by Stern, Bedford, and Millwater.[2] Also included were the results of a comprehensive compilation of shallow grazing angle backscatter data. The compilation suggested, for some sediments, the possible importance of a new hypothetical mechanism for backscatter: resonant scattering from trapped bubbles. A preliminary model for acoustic backscatter from a spatial distribution of trapped bubbles in sediment was then presented.

This report contains improvements to the bubble backscatter model, including: (1) a method for modeling spherical acoustic sources in the water column, (2) incorporation of the Biot model in describing acoustic propagation through the sediment, and (3) an improved estimate of the trapped bubble size distribution function. This new model begins with a calculation of the pore pressure in the sediment, given a spherical acoustic source in the water column. This procedure is discussed in Section 2. Section 3 then describes how the backscattering strength of the sediment is computed. In Section 4, the resulting theoretical model is compared with experiment. A discussion of the results follows in Section 5.

This page intentionally left blank.

2. PORE PRESSURE

In this report we consider the pressure field generated by a point source in the water column above a sediment boundary, illustrated in Fig. 2.1. Of interest is the fluid pressure in the interstitial pores. This problem is treated by decomposing the spherical wavefield into a spectrum of plane waves. The technique follows the treatments of Brekhovskikh[3] and Westwood.[4] A Biot penetration model is used to calculate the transmission coefficient for each plane wave. The pore pressure is then obtained by summing the contributions of all plane waves.

2.1 PLANE WAVE DECOMPOSITION

The linear acoustic wave equation in a homogeneous medium with sound speed c is

$$\nabla^2 p = \frac{1}{c^2}\frac{\partial^2 p}{\partial t^2} \quad . \tag{2.1}$$

The solution to the above equation that describes the pressure field caused by a spherical source is

$$p = p_0 \frac{e^{i(kR - \omega t)}}{R} \quad , \tag{2.2}$$

where R is the distance from the source, p_o the pressure amplitude at unit distance, t the time, ω the angular frequency, and $k=\omega/c$ the acoustic wave number. If the source is placed at the origin of a rectangular coordinate system, the distance R is given by $R=(x^2+y^2+z^2)^{1/2}$. If we set p_o to unity, suppress the time dependence $e^{-i\omega t}$, and confine ourselves to the z=0 plane, the pressure field can be written as

$$p(x,y) = \frac{e^{ikr}}{r} \quad , \tag{2.3}$$

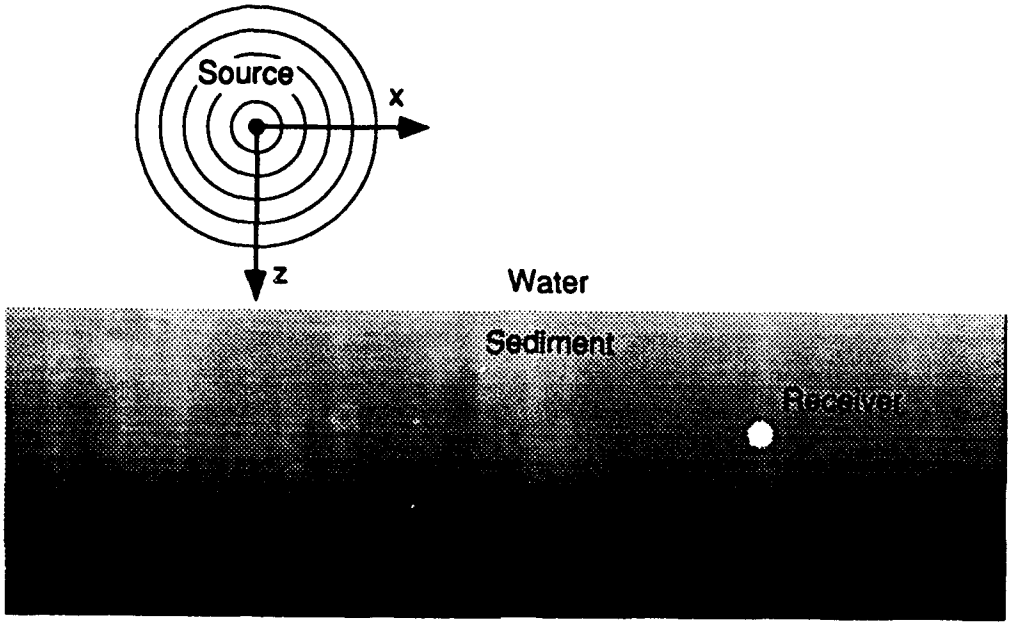

FIGURE 2.1
SPHERICAL SOURCE ABOVE WATER-SEDIMENT BOUNDARY

ARL - UT
AS-93-464
NPC/RFO
8-93/hd2

where $r=(x^2+y^2)^{1/2}$.

The pressure field can now be expanded in a double Fourier integral in the variables x and y,

$$\frac{e^{ikr}}{r} = \int\int A(k_x,k_y)\, e^{i(k_x x+k_y y)}\, dk_x dk_y \qquad (r \neq 0) \quad , \qquad (2.4)$$

where $A(k_x,k_y)$ is given by

$$(2\pi)^2 A(k_x,k_y) = \int\int \left(\frac{e^{ikr}}{r}\right) e^{-i(k_x x+k_y y)}\, dk_x dk_y \quad . \qquad (2.5)$$

The above integral is more tractable in polar coordinates:

$$\begin{aligned} k_x &= q\cos\psi \\ k_y &= q\sin\psi \\ q &= (k_x^2+k_y^2)^{1/2} \\ x &= r\cos\phi \\ y &= r\sin\phi \\ dx\,dy &= r\,dr\,d\phi \quad . \end{aligned}$$

In this coordinate system $A(k_x,k_y)$ is given by

$$(2\pi)^2 A(k_x,k_y) = \int_0^{2\pi}\int_0^{\infty} e^{ir[k-q\cos(\phi-\theta)]}\, dr\, d\phi$$

$$= \int_0^{2\pi} \left[\frac{e^{ir[k-q\cos(\phi-\theta)]}}{i[k-q\cos(\phi-\theta)]}\right]_{r=0}^{r=\infty} d\phi \quad . \qquad (2.6)$$

If there is some absorption, even if it is vanishingly small, k will have a positive imaginary part. In this case the quantity in brackets is zero when r = infinity. Therefore

$$(2\pi)^2 A(k_x,k_y) = \int_0^{2\pi} \frac{i\, d\phi}{[k - q\cos(\phi - \theta)]}$$

$$= \frac{i}{k}\int_0^{2\pi} \frac{d\phi}{[1 - \frac{q}{k}\cos(\phi - \theta)]} \quad . \qquad (2.6)$$

The integral in Eq. (2.6) is tabulated.[5] Upon substituting into Eq. (2.6), the following expression for $A(k_x,k_y)$ is obtained:

$$A(k_x,k_y) = \frac{i}{2\pi\sqrt{k^2 - k_x^2 - k_y^2}} \quad . \qquad (2.7)$$

Substitution of Eq. (2.7) into Eq. (2.4) yields

$$p(x,y) = \int_{-\infty}^{\infty}\int_{-\infty}^{\infty} \frac{i}{2\pi\sqrt{k^2 - k_x^2 - k_y^2}} e^{i(k_x x + k_y y)}\, dk_x dk_y \quad . \qquad (2.8)$$

The above expression for the pressure field in the z=0 plane can be generalized to describe the field in all space. This is done by multiplying the integrand by $e^{ik_z z}$ for z>0 or by $e^{-ik_z z}$ for z<0.

$$p(x,y,z) = \int_{-\infty}^{\infty}\int_{-\infty}^{\infty} \frac{i}{2\pi\sqrt{k^2 - k_x^2 - k_y^2}} e^{i(k_x x + k_y y + k_z z)}\, dk_x dk_y \ , \quad (z \geq 0) \qquad (2.9)$$

$$p(x,y,z) = \int_{-\infty}^{\infty}\int_{-\infty}^{\infty} \frac{i}{2\pi\sqrt{k^2 - k_x^2 - k_y^2}} e^{i(k_x x + k_y y - k_z z)}\, dk_x dk_y \ , \quad (z \leq 0) \qquad (2.10)$$

where

$$k_z = \sqrt{k^2 - k_x^2 - k_y^2} \quad . \qquad (2.11)$$

This "continuation" is justified because the integrand still satisfies the wave equation and because the new expressions reduce to the original expression Eq. (2.8) for the z=0 plane when z approaches zero.

The integrals in Eq. (2.9) and Eq. (2.10) are over the entire $k_x k_y$ plane. In order to span this plane, according to Eq. (2.11), imaginary values of k_z must be included. These so-called "inhomogeneous waves" attuenuate exponentially with spatial dimension z and must be included to complete the construction of a spherical wavefield with plane waves.

In order to evaluate the integrals, Eq. (2.9) and Eq. (2.10), a transformation to spherical coordinates is made, as shown in Fig 2.2:

$$\begin{aligned} k_x &= k \sin\theta \cos\phi \quad , \\ k_y &= k \sin\theta \sin\phi \quad , \\ k_z &= k \cos\theta \quad . \end{aligned} \tag{2.12}$$

In the transformation the elemental area on the $k_x k_y$ plane becomes

$$dk_x dk_y = (k \sin\theta \, d\phi)(k \cos\theta \, d\theta) \quad . \tag{2.13}$$

In order to cover the entire plane, ϕ goes from 0 to 2π. By allowing θ to run from 0 to $\pi/2$, a disk on the plane of radius k is covered. In order to span the rest of the plane, q is further allowed to vary between $\pi/2$ and $\pi/2$-i∞. It would also have been possible to span the plane by letting q vary between $\pi/2$ and $\pi/2$+i∞, but this would have made the inhomogeneous waves *increase* in amplitude with increasing z instead of attenuating.

In the new coordinates, Eq. (2.9) becomes

$$p(x,y,z) = \frac{ik}{2\pi} \int_{\theta=0}^{\frac{\pi}{2} - i\infty} \int_{\phi=0}^{2\pi} e^{i(k_x x + k_y y + k_z z)} \sin\theta \, d\phi \, d\theta \quad , \quad (z \geq 0) \quad . \tag{2.14}$$

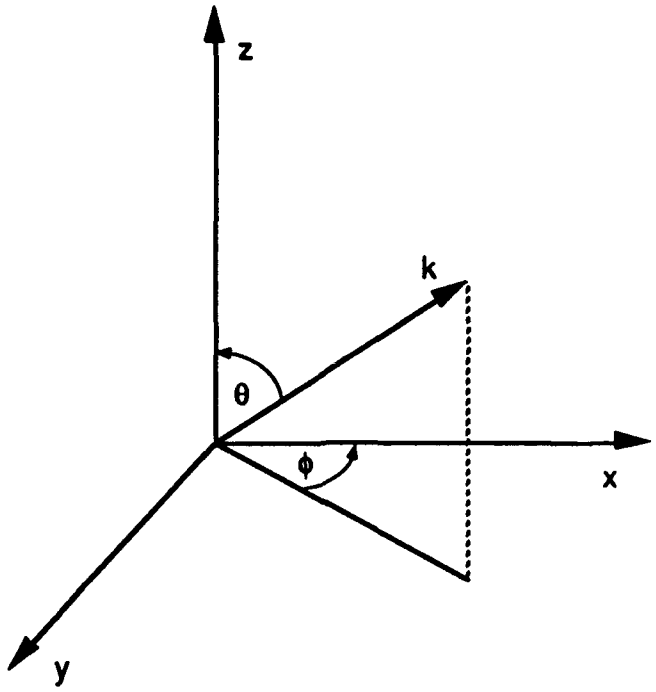

FIGURE 2.2
EXPRESSION OF WAVENUMBER k IN RECTANGULAR COORDINATES

ARL - UT
AS-93-465
NPC/RFO
8-93/hd2

In order to determine the pressure field below the sediment interface, as in Fig. 2.3, each plane wave component must be multiplied by an appropriate plane wave transmission coefficient. The resulting pressure is given by

$$p(x,y,z) = \frac{ik}{2\pi}\int_{\theta=0}^{\frac{\pi}{2}-i\infty}\int_{\phi=0}^{2\pi} e^{i(k_x x+k_y y+k_z z_1+k_{zs} z_2)} W(\theta)\sin\theta\, d\phi\, d\theta\,, \quad (z \geq 0) \quad , \quad (2.15)$$

where W is the transmission coefficient, which depends on the angle of incidence θ. z_1 is the height of the source, z_2 is the depth of the receiver, and k_{zs} is the wavenumber in the lower medium. It can be shown that the integral over ϕ is a Bessel function. This is done by first expressing the variables x and y in polar coordinates:

$$x = r\cos\phi_1\,, \quad y = r\sin\phi_1 \quad . \qquad (2.16)$$

The integral over ϕ can now be written as

$$\begin{aligned}\int_{\phi=0}^{2\pi} e^{i(k_x x+k_y y}d\phi &= \int_{\phi=0}^{2\pi} e^{ikr\sin\theta(\cos\phi_1\cos\phi+\sin\phi_1\sin\phi)}d\phi \\ &= \int_{\phi=0}^{2\pi} e^{ikr\sin\theta[\cos\phi_1\cos(\phi-\phi_1)]}d\phi \\ &= 2\pi J_0(kr\sin\theta) \quad .\end{aligned} \qquad (2.17)$$

By combining Eq. (2.14) and Eq. (2.16), a simplified expression for the pressure is obtained:

$$p(x,y,z) = \int_{\theta=0}^{\frac{\pi}{2}-i\infty} J_0(kr\sin\theta)\, e^{i(k_z z_1+k_{zs} z_2)} W(\theta)\sin\theta\, d\theta \quad . \qquad (2.18)$$

2.2 INCORPORATION OF BIOT MODEL

In order to solve Eq. (2.18) for the pressure below the sediment boundary, the transmission coefficient $W(\theta)$ and vertical wavenumber k_{zs} in the sediment must be specified. For this purpose the Biot penetration model

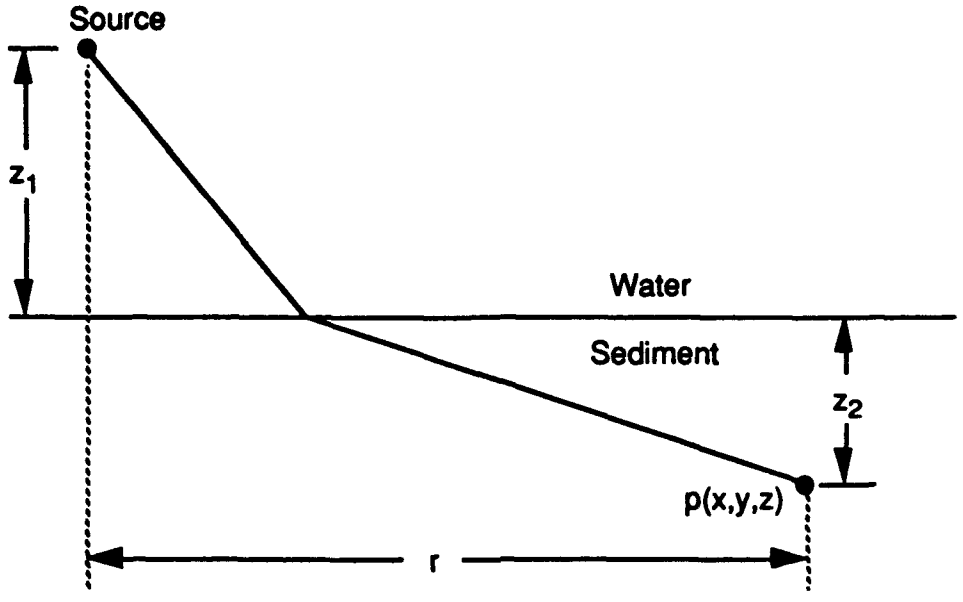

FIGURE 2.3
PRESSURE FIELD BELOW WATER-SEDIMENT INTERFACE

ARL - UT
AS-93-466
NPC/RFO
8-93/hd2

described in ARL-TR-92-12[6] was used. This model was originally developed by Stern, Bedford, and Millwater[7] and later modified to treat gassy sediments. This was done by varying the complex compressibility and density of the pore fluid. The gas contribution to these parameters was obtained using a theory developed by Hawkins[8] involving reflection coefficients from bubble distributions.

The Biot model differs from traditional ways of treating acoustic media in that it allows for two phases: a solid skeletal phase through which a fluid phase is allowed to flow freely. It is based on the following coupled pair of equations of motion:

$$\mu\nabla^2\mathbf{u} + (H-2\mu)\nabla(\nabla\cdot\mathbf{u}) - C\nabla(\nabla\cdot\mathbf{w}) = \rho\ddot{\mathbf{u}} - \rho_f\ddot{\mathbf{w}} \tag{2.19}$$

$$C\nabla(\nabla\cdot\mathbf{u}) - M\nabla(\nabla\cdot\mathbf{w}) = \rho_f\ddot{\mathbf{u}} - (c\rho_f/\beta)\ddot{\mathbf{w}} - (F\eta/\kappa)\dot{\mathbf{w}} \quad , \tag{2.20}$$

where **u** and **w** are the fluid and solid displacements, μ is the fluid viscosity, ρ_f and ρ are the mass densities of fluid and saturated sediment, respectively, k is the permeability, and F is a constant that accounts for the frequency dependence of the drag force between fluid and solid. The constants H, C, and M are determined by the compressibilities of the fluid and solid constituents.

One important feature of the Biot model is that it predicts two compressional waves in the medium, in addition to a shear wave. For the faster of these waves, the fluid moves generally in phase with the solid part of the medium. For the slow wave the two components move out of phase. Usually the slow waves can be neglected and single phase models can be used to model ocean sediments. Under certain conditions, however, slow waves appear to be dominant. Such is the case when a wavefront is incident upon a sediment half space at a grazing angle less than the critical angle for the fast wave.

The above described Biot penetration model calculates, for any complex angle of incidence θ, the pore pressure transmission coefficient $W(\theta)$ and vertical wavenumber k_{zs}. The transmission coefficient $W(\theta)$ is obtained from

simultaneous solution of equations (51-54) of Stern *et al.* The fast and slow vertical wavenumbers k_{zs} are given by Eq. (59) and Eq. (60), respectively.

Equation (2.18) is then calculated numerically, given $W(\theta)$ and k_{zs}. Figure 2.4 is a plot of the computed pore pressure in the sediment, given the input parameters of Table 2.1. The pressure contributions are broken down according to the types of waves involved. Wavespeeds of 1690 m/s for the fast wave and 1170 m/s for the slow wave are predicted, with attenuations of 12.2 and 41.2 dB/m, respectively. It is clear that the slow wave has a pressure amplitude that is not negligible in comparison to that of the fast wave, particularly when the horizontal distance to the acoustic source is large. Hence the effects of the slow wave must be included in predicting total pressures in the sediment as well as backscattered pressures from the sediment.

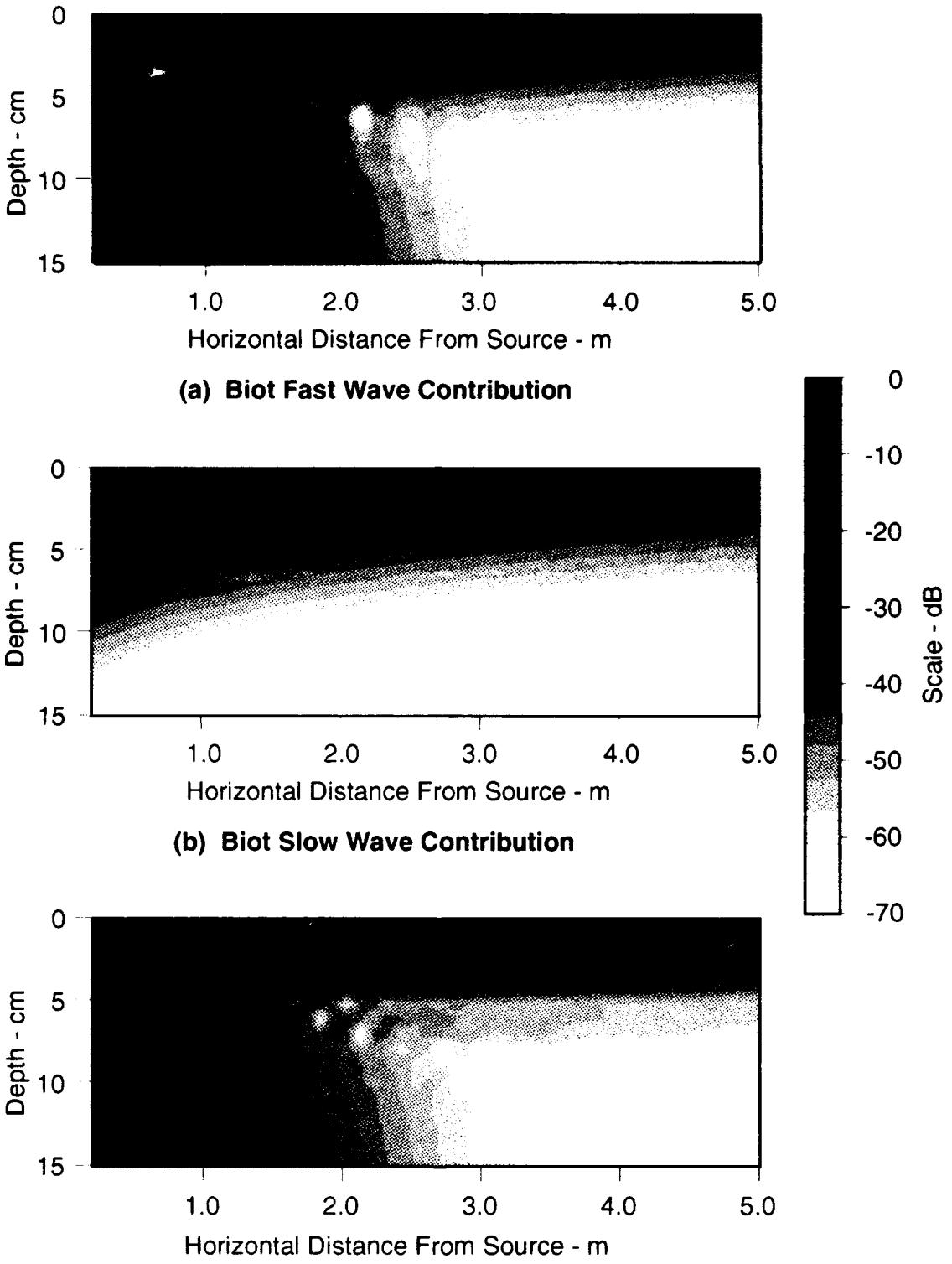

FIGURE 2.4
PORE PRESSURES DUE TO 30 kHz SPHERICAL SOURCE AT HEIGHT OF 50 cm ABOVE BOTTOM

TABLE 2.1
PENETRATION MODEL INPUT PARAMETERS

Fluid Density	1000	kg/m^3
Fluid Bulk Modulus	2.0×10^9	Pa
Porosity	0.4	
Grain Density	2650	kg/m^3
Pore Size	1.0×10^{-5}	m
Viscosity	1.0×10^{-3}	kg/m-s
Permeability	1.0×10^{-10}	m^2
Grain Bulk Modulus	9.0×10^9	Pa
Frame Shear Modulus	2.61×10^7	Pa
Shear Logarithmic Decrement	0.15	
Frame Bulk Modulus	4.36×10^9	Pa
Bulk Logarithmic Decrement	0.15	
Virtual Mass Parameter	1.25	
Gas Bulk Modulus	2.48×10^5	Pa
Bubble/Pore Radius Ratio	0.06	
Gas Content	0	

3. SEDIMENT BACKSCATTERING STRENGTH

3.1 CALCULATION OF BACKSCATTERING STRENGTH BY RECIPROCITY

Consider the situation illustrated in Fig. 3.1. In Appendix A an approximation for the backscattered pressure amplitude p_2 at A from a scatterer at B is derived:

$$p_2 = \sqrt{\frac{\sigma}{4\pi}}\,\frac{p_1^2}{p_0} \quad , \tag{3.1}$$

where σ is the effective cross section of the scatterer, defined as the area which, when multiplied by the incident intensity, equals the total scattered power. The incident pressure amplitude generated by the source at a distance of 1 m in the water column is p_0, and p_1 is the pressure generated at the scatterer, located at B.

In this analysis, the sediment is a medium with many scatterers throughout its volume. A mean scattering cross section per unit volume σ_{bv} can be computed, given the scattering cross sections and population densities of the contained scatterers. If a projector at A insonifies a volume element dxdydz at B, the returned pressure at A is

$$p_2 = \sqrt{\frac{\sigma_{bv}\,dxdydz}{4\pi}}\,\frac{p_1^2}{p_0} \quad . \tag{3.2}$$

The scattering can be treated as a function of location along the water-sediment interface, as in Fig. 3.2. In this case, the backscattered intensity from a surface element dxdy is the sum of all backscatter contributions from the sediment volume below the surface element dxdy. The total mean square backscattered pressure per unit surface area is given by

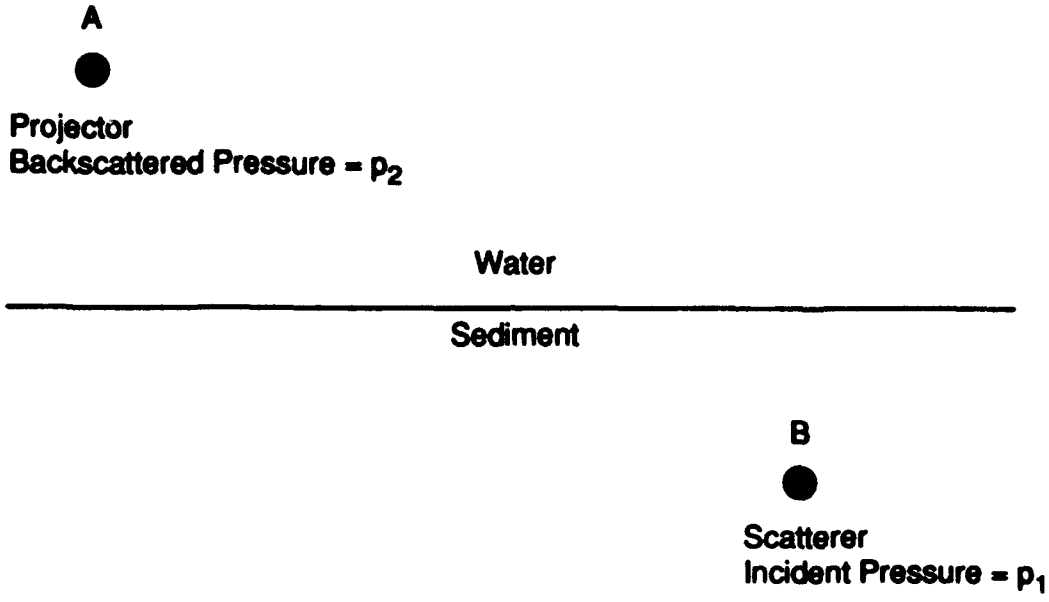

FIGURE 3.1
BACKSCATTER AT A FROM SINGLE SCATTERER AT B

ARL - UT
AS-93-466
NPC/RFO
8-93/hd2

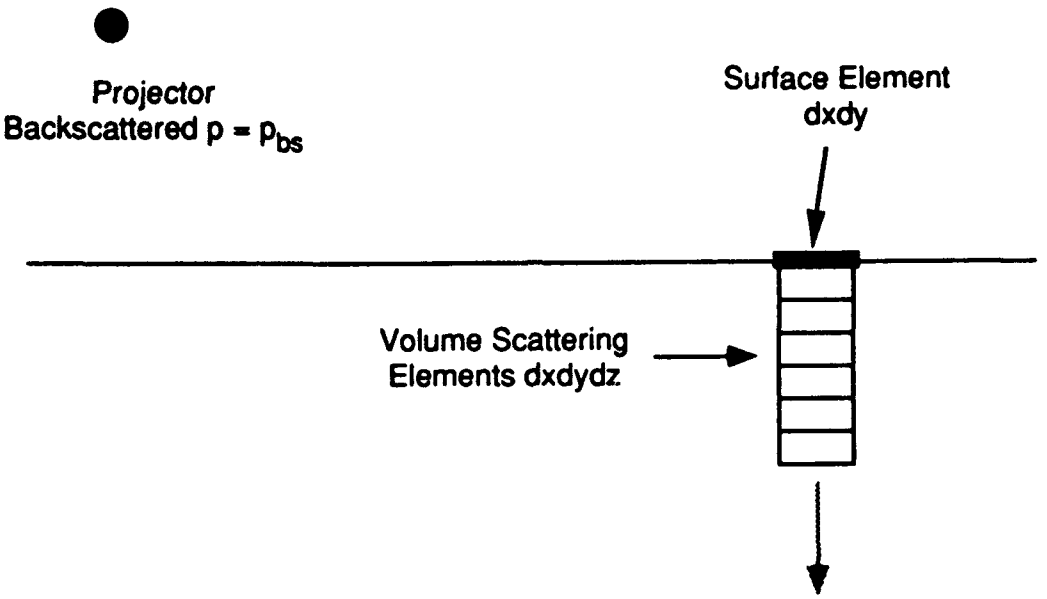

FIGURE 3.2
BACKSCATTER FROM THE VOLUME
BELOW SURFACE ELEMENT dxdy

ARL - UT
AS-93-469
NPC/RFO
8-93/hd2

$$p_{bs}^2 = \int_0^{\infty} \frac{\sigma_{bv}}{4\pi} \frac{p_1^4}{p_0^2} dz \quad . \tag{3.3}$$

Figure 3.3 illustrates the computation of the backscattering strength of a surface element. The backscattering strength is

$$BS = 10 \log \left(\frac{p_s^2}{p_o'^2} \right) \quad , \tag{3.4}$$

where p_s is the root mean square scattered pressure at unit radius from the surface element and p_o' is the incident pressure at the surface element. The incident pressure p_o' is

$$p_o' = p_o / R \quad , \tag{3.5}$$

where R is the distance from the source to the surface element. The scattered pressure at unit radius is obtained from the scattered pressure p_{bs} at the source,

$$p_s = p_{bs} R \quad . \tag{3.6}$$

By combining Eqs. (3.3) - (3.6), the backscattering strength is expressible as a function of σ_{bv}, R, p_o, and p_1.

$$BS = 10 \log \frac{R^4}{4\pi p_o^4} \int_o^{\infty} \sigma_{bv} p_1^4 \, dz \quad . \tag{3.7}$$

3.2 DETERMINATION OF SEDIMENT VOLUME SCATTERING CROSS SECTION σ_{bv}

In order to find the backscattering strength via Eq. (3.7), it is necessary to calculate σ_{bv}, the backscattering cross section per unit volume of sediment.

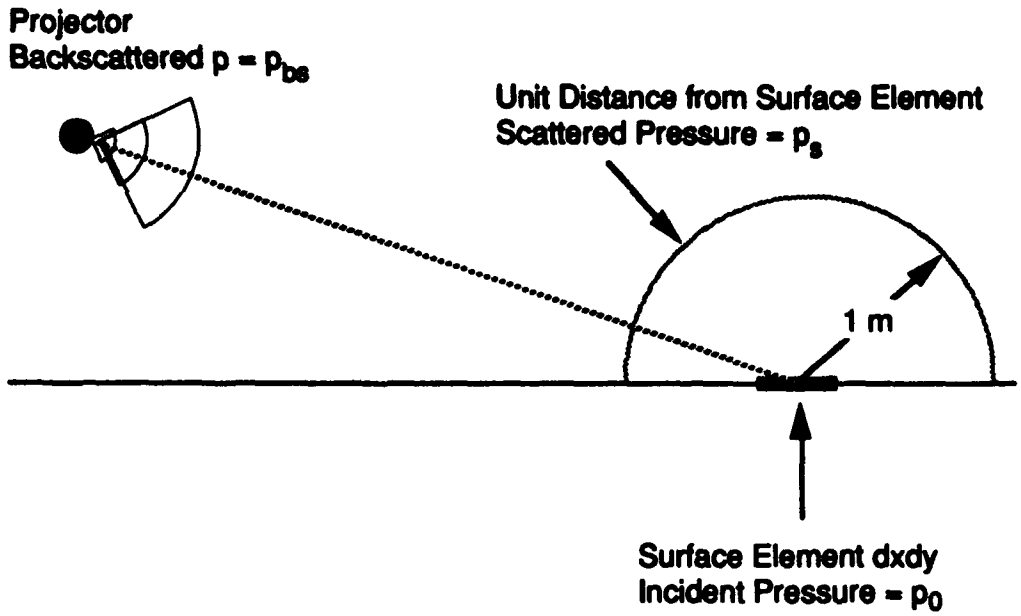

FIGURE 3.3
CALCULATING THE BACKSCATTERING STRENGTH
FROM SURFACE ELEMENT dxdy

Since the hypothetical mechanism for scattering in this model is bubble resonant backscatter, σ_{bv} can be expressed as follows:

$$\sigma_{bv} = \int_0^\infty f_b(r_b)\, \sigma(r_b)\, dr_b \quad , \tag{3.8}$$

where $f_b(r_b)$ is the spatial distribution function of bubbles, defined as the number of bubbles per unit volume per unit radius increment about the radius r_b, and $\sigma(r_b)$ is the scattering cross section of a single bubble of radius r_b. Expressions for $\sigma(r_b)$ and $f_b(r_b)$ are developed in subsections 3.2.1 and 3.2.2.

In developing the model, three assumptions are made:

(1) A bubble's size is regulated by the pore in which it is found; i.e., the ratio of bubble radius to pore radius is constant. This assumption is necessary to permit an estimate of the bubble size distribution in the absence of other information.

(2) The possibility of multiple scattering between bubbles is neglected. Justifcation for this assumption is included in Appendix B.

(3) The bubbles act as though they were spherical, isolated, and surrounded by water. The effects of the interaction between bubbles and between bubbles and the walls of the pores are neglected.

There is some experimental and theoretical support for this approximation. Howkins[9] predicted and measured the resonance frequencies of bubbles near rigid boundaries. Two configurations were studied, one involving a bubble near a semi-infinite rigid plane and another involving a bubble contained inside a rigid cylindrical cup. In neither case was there a dramatic influence on the bubble's resonance frequency. Resonance frequencies decreased by 15% for the plane boundary and 50% for the cylindrical cup. A bubble

trapped between sand grains might act similarly, being more confined than a free bubble near a semi-infinite plane but less confined than one inside a cylindrical cup.

3.2.1 Estimate of Single Bubble Backscattering Cross Section

Equation (3.8) requires that $\sigma(r_b)$, the single bubble backscattering cross section, be specified. The scattering cross section for a single spherical bubble of radius r_b insonified by a signal of frequency f is given by Wildt:[10]

$$\sigma_r(r_b) = \frac{4\pi r_b^2}{\left[\left(\frac{f_r}{f}\right)^2 - 1\right]^2 + \delta^2} \quad . \tag{3.9}$$

δ is a damping constant and f_r is the resonance frequency, given by Minneart[11]

$$f_r = \frac{1}{2\pi r_b}\left(\frac{3\gamma P}{\rho}\right)^{1/2} \quad , \tag{3.10}$$

where γ, P, and ρ are the ratio of specific heats, pressure, and density, respectively, of the medium inside the bubble. Medwin[12] showed that, for resonant bubbles, $r_b f_r$ is approximately 3 and δ is approximately 0.1. It is convenient to work in terms of the variable $v = \ln(r_b)$ instead of r_b. In this notation the single bubble scattering cross section is

$$\sigma_v(v) = \frac{4\pi e^{2v}}{\left[\left(\frac{f_r}{f}\right)^2 - 1\right]^2 + \delta^2} \quad . \tag{3.11}$$

3.2.2 Estimate of Bubble Size Distribution

Equation (3.8) requires that the bubble size distribution function $f_b(r_b)$ be specified. Our approach is to first obtain a pore volume distribution function. A

bubble distribution function is then found by assuming that bubbles always occupy a constant fraction of the available pore space, in accordance with assumption (1) stated previously.

Pore Size Distribution Function

Finney and Wallace[13] investigated the formation of pores between randomly packed identical spheres. Figure 3.4 is a histogram of the distribution of interstitial pore radii for an aggregate of spheres. It can be approximated as a bimodal distribution function p(x,y) where x and y are the natural logarithms of the grain and pore radii, respectively. For any value of x, p(x,y) is approximated by a sum of two normal distributions.

$$p(x,y) = A\left[\frac{1}{\sqrt{2\pi}\,b_1} e^{-(y-x-a_1)^2/2b_1^2}\right] + B\left[\frac{1}{\sqrt{2\pi}\,b_2} e^{-(y-x-a_2)^2/2b_2^2}\right] \quad , \quad (3.12)$$

where a_i is the mean and b_i is the standard deviation of the ith peak.

Sediments have a measurable particle size distribution function $f_x(x)$, where x = log(grain radius). A pore size distribution function $f_p(y)$ is estimated by convolving this function with p(x,y):

$$f_p(y) = f_x(x)^* p(x,y) \quad . \quad (3.13)$$

In writing Eq. (3.13) we are neglecting the possibility that particles of varying sizes pack differently than those of a single size. For example, small particles may occupy the pores created between larger particles. An assumption is also made that irregular sediment grains pack like perfect spheres. The justification behind proceeding with these assumptions comes from the measured porosities of sandy sediments. Porosities between 0.36 and 0.4 are common for sandy sediments. This compares closely with a porostiy of 0.363 for randomly packed identical spheres.[14]

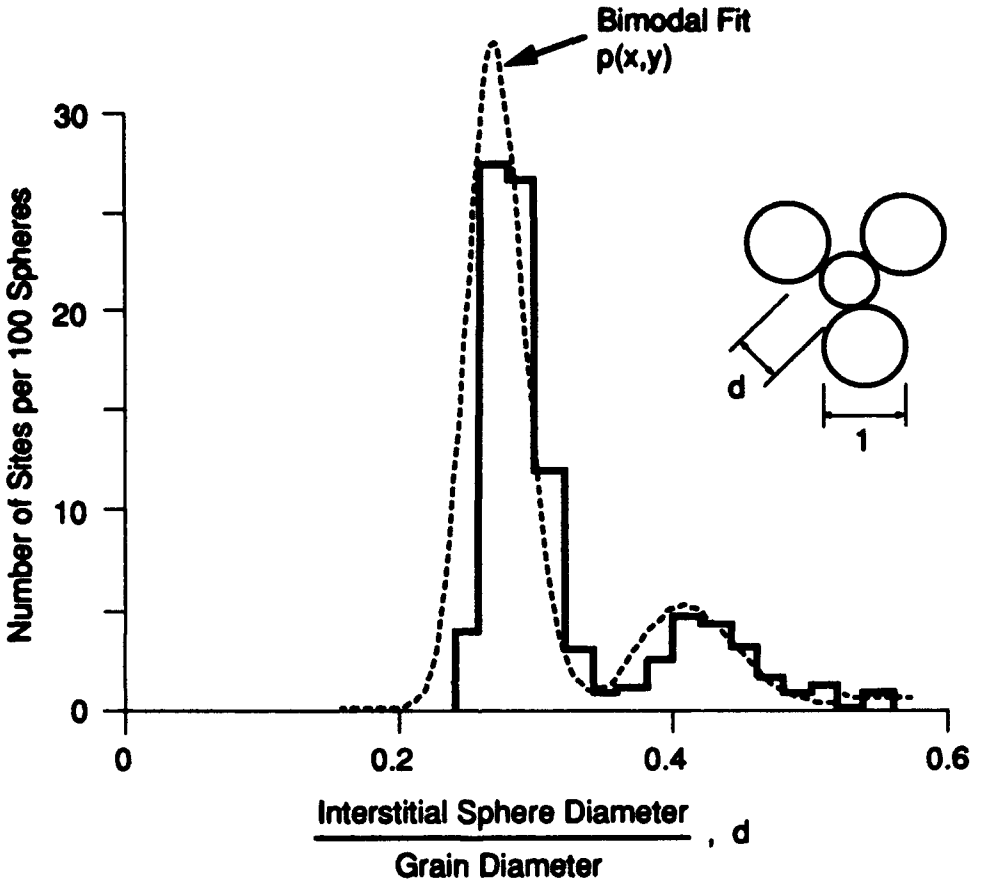

FIGURE 3.4
DISTRIBUTION OF INTERSTITIAL SPHERE SIZES FOR DENSE RANDOM PACKING OF HARD SPHERES OF UNIT DIAMETER

ARL - UT
AS-93-471
NPC/RFO
8-93/hd2

Bubble Size Distribution Function

Assumption (1) states that a bubble's radius is governed by the size of the surrounding pore. This means that the bubble size distribution $f_b(v)$, where v is the natural log of the bubble radius, will reflect the pore size distribution $f_p(v)$:

$$f_b(z) = \xi f_p(v - \ln(R_{bp})) \quad . \tag{3.14}$$

R_{bp} is a constant equal to the ratio of a bubble's radius to that of its surrounding pore. It is assumed that each pore may hold only one gas bubble, and that the fraction of pores that indeed have gas bubbles is ξ. In the absence of any further information, it will be assumed that ξ is a constant independent of pore size. The gas fraction ζ is obtainable by dividing the total volume of bubbles by the porosity:

$$\zeta = \frac{\int_{-\infty}^{\infty} \frac{4}{3}\pi e^{3v} f_b(v)\, dv}{\beta} \quad . \tag{3.15}$$

In this analysis R_{bp} and ζ are treated as free parameters and are varied to fit the model to experimental data.

4. COMPARISON OF THEORY WITH EXPERIMENT

In Fig. 4.1 comparisons are made between the predictions of the backscatter model and experimental measurements of the backscattering strength taken over three selected sites. The input parameters for each site are listed in Table 4.1. In each case a best fit was obtained by varying the gas fraction ζ and the bubble-to-pore radius ratio R_{bp}. The resulting gas fractions are annotated and varied between 1×10^{-5} and 3×10^{-6}.

The model predicts a peak in the backscattering strength at a frequency that corresponds to resonance for the bubbles in the distribution. The width of this peak will depend on the width of the bubble size distribution. The backscattering strength will decrease with increasing frequencies that are greater than resonance. In this respect the model differs from other current models, which always predict an increase in backscattering strength with increasing frequency.

At present the model is still being developed and these results must be regarded as preliminary. An impoved estimate of the compressibility of the gassy fluid phase is being developed. An estimate of the acoustic impedance of the fluid constrained in the sediment pores is also being incorporated. These changes to the model will probably change the amplitudes of the predicted backscattering strengths in Fig. 4.1. The overall features, i.e., the broad maximum in backscattering strength at bubble resonance and the model's sensitivity to very small gas fractions, are not expected to change.

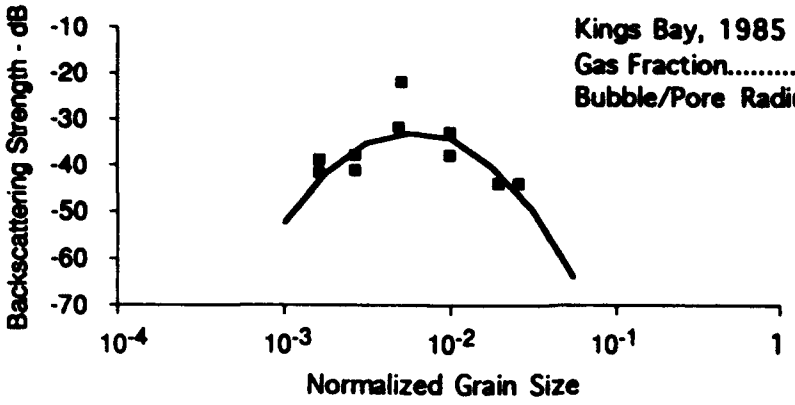

Kings Bay, 1985
Gas Fraction.....1.0×10^{-5}
Bubble/Pore Radius Ratio (Rbp)...0.06

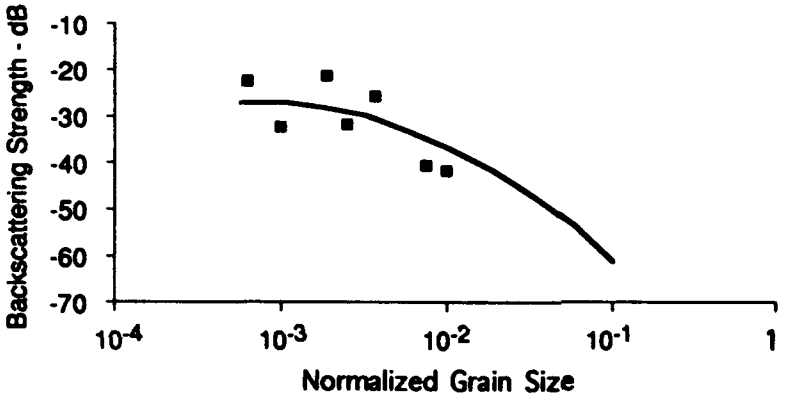

Panama City, 1986
Gas Fraction.....3×10^{-6}
Rbp.....0.1

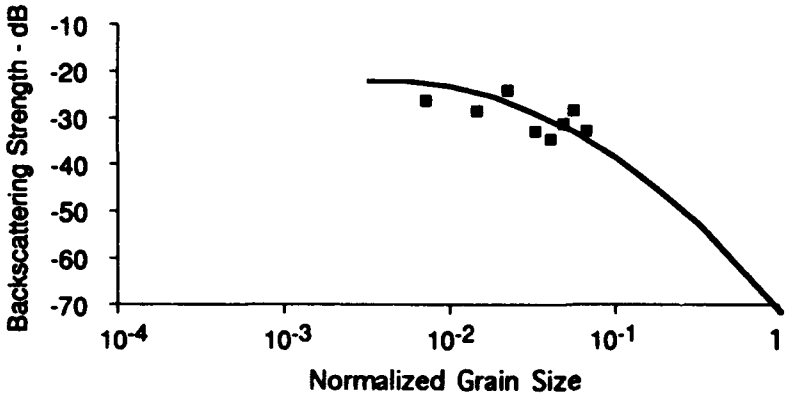

Jacksonville, 1989
Gas Fraction.....2×10^{-5}
Rbp.....0.01

FIGURE 4.1
COMPARISON OF EXPERIMENTAL DATA WITH BACKSCATTERING STRENGTHS PREDICTED BY EQ. (3.7)

ARL - UT
AS-93-472
NPC/RFO
8-93/hd2

TABLE 4.1
BACKSCATTER MODEL INPUT PARAMETERS

Site		Kings Bay 1985	Panama City 1986	Jacksonville 1989
Fluid Density	(kg/m^3)	1000	1000	1020
Fluid Bulk Modulus	(Pa)	2.25×10^{9}	2.25×10^{9}	2.406×10^{9}
Porosity		0.3633	0.3906	0.3793
Grain Density	(kg/m^3)	2656	2650	2650
Grain Radius	(m)	3.896×10^{-4}	1.593×10^{-4}	5.586×10^{-4}
Viscosity	(kg/m-s)	1.0×10^{-3}	1.0×10^{-3}	1.0×10^{-3}
Permeability	(m^2)	1.0×10^{-10}	1.0×10^{-10}	1.0×10^{-10}
Grain Bulk Modulus	(Pa)	9.0×10^{9}	9.0×10^{9}	1.06×10^{10}
Frame Shear Modulus	(Pa)	2.61×10^{7}	2.61×10^{7}	2.57×10^{7}
Shear Log Decrement		0.15	0.15	0.15
Frame Bulk Modulus	(Pa)	4.36×10^{9}	4.36×10^{9}	4.36×10^{9}
Bulk Log Decrement		0.15	0.15	0.15
Virtual Mass Parameter		1.25	1.25	1.25
Gas Bulk Modulus	(Pa)	2.48×10^{5}	2.48×10^{5}	2.48×10^{5}
Bubble/Pore Radius Ratio		0.06	0.1	0.01
Gas Content		1.0×10^{-5}	3×10^{-6}	2×10^{-5}

This page intentionally left blank.

5. CONCLUSION

A heuristic model for high frequency acoustic backscatter from sandy sediments based on bubble resonance behavior has been developed. This model is consistent with the broad backscattering strength maximum observed in some of the experimental data and demonstrates that a trapped bubble backscattering mechanism may be significant in high frequency acoustic backscatter from sediments.

The analysis demonstrates that gas bubbles are a likely cause of observed backscatter from sediments. Very small gas fractions of between 1×10^{-5} and 3×10^{-6} are necessary. Since there is no direct way to measure gas fractions this small, an independent verification of this analysis is required, which is difficult.

The assumption that the bubble size is proportional to the pore size was made to allow a first estimate of the bubble size distribution. Further research is required to determine a more precise relationship between pore geometry and bubble size.

The effects of Biot slow and fast compressional waves have been included. The results show that at very shallow grazing angles the slow wave's amplitude is significant in comparison to that of the fast wave. This suggests that a complete description of shallow grazing angle penetration must include the effects of the slow wave. For this reason the Biot theory appears to be most appropriate in acoustic modeling in this regime.

At present, work is in progress in improving the backscatter model. An expression for the backscattering cross section for trapped bubbles is being developed. This will allow elimination of the assumption that trapped bubbles scatter as though they existed in an unbounded medium. Further improvements will include studies of grain packing structures and their relationships to trapped bubble sizes and geometries.

This page intentionally left blank.

APPENDIX A
RECIPROCITY PRINCIPLE

This page intentionally left blank.

Consider the situation illustrated in Fig. A.1. According to the reciprocity principle, the sound pressure at B when a source is placed at A is the same as that produced at A when the same source is placed at B. In the case where sound from a source at A encounters a scatterer at B, the scatterer can be regarded as another source whose sound pressure can be measured back at A. In this case, a signal propagating along the return path experiences the same loss that the original incident signal did on its way to B. Let a cw source at A cause a complex pressure $\mathbf{p_1}$ to exist at B. The scatterer at B will return a complex pressure $\mathbf{p_2}$ at A, given by:

$$\mathbf{p_2} = (\mathbf{p_1}\,\zeta)\left(\frac{\mathbf{p_1}}{\mathbf{p_0}}\right) \quad , \tag{A.1}$$

where $\mathbf{p_1}\zeta$ is the pressure generated by the scatterer, measured at a unit distance from the scatterer. The incident pressure generated by the source at a distance of 1 m in the water column is $\mathbf{p_0}$. $\zeta = re^{i\theta}$ is a complex factor related to the scattering cross section. Let the time dependent complex pressures $\mathbf{p_0}$, $\mathbf{p_1}$, $\mathbf{p_2}$ be expressed as

$$\begin{aligned} \mathbf{p_0} &= p_0 e^{i(\theta_\sigma - \omega t)} \\ \mathbf{p_1} &= p_1 e^{i(\theta_i - \omega t)} \\ \mathbf{p_2} &= p_2 e^{i(\theta_r - \omega t)} \quad , \end{aligned} \tag{A.2}$$

where p_1, p_2, and p_3 are moduli and θ_1,θ_2, and $\alpha\nu\delta$ θ_3 are phases of the complex pressures $\mathbf{p_0}$, $\mathbf{p_1}$, and $\mathbf{p_2}$. Upon substitution into Eq. (A.1),

$$p_2 e^{i(\theta_r - \omega t)} = \left(p_1 e^{i(\theta_i - \omega t)} re^{i\theta}\right)\left(\frac{p_1 e^{i(\theta_i - \omega t)}}{p_0 e^{i(\theta_\sigma - \omega t)}}\right) \quad . \tag{A.3}$$

Upon taking a time average of Eq. (A.3),

FIGURE A.1
BACKSCATTER AT A FROM SINGLE SCATTERER AT B

$$p_2 \langle e^{i(\theta_2 - \omega t)} \rangle = r \frac{p_1^2}{p_0} \langle e^{i(\theta + 2\theta_1 - \theta_0 - \omega t)} \rangle \quad . \tag{A.4}$$

The factor r is related to the scattering cross section σ as follows:

$$r = \sqrt{\frac{\sigma}{4\pi}} \quad , \tag{A.5}$$

where σ is defined as the area which, when multiplied by the incident intensity, equals the total scattered power. Upon substituting Eq. (A.5) into Eq. (A.4) and noting that the time averages of the bracketed quantities in Eq. (A.4) are unity,

$$p_2 = \sqrt{\frac{\sigma}{4\pi}} \frac{p_1^2}{p_0} \quad . \tag{A.6}$$

The situation in Fig. 3.1 differs from that in Fig. A.1 in that the scatterer exists under a fluid-sediment boundary. The above derivation leading up to Eq. (A.6) rests on the assumption that both scatterer and projector exist in the same medium. For the case in which the scatterer is below a sediment boundary, an impedance mismatch between fluid and sediment must be accounted for. In this analysis, such a mismatch is neglected. As a result, Eq. (A.6) can only be considered an approximation. The approximation should be reasonable since the trapped bubbles that act as scatterers exist in the trapped fluid within the sediment pores. Effectively, the assumption is being made that the interstitial fluid has the same acoustic impedance as the fluid above the sediment.

This page intentionally left blank.

APPENDIX B
JUSTIFICATION OF SINGLE SCATTERING MODEL

This page intentionally left blank.

Attenuation in sediment is caused by absorption and scattering of an incident acoustic wave. The single scattering approximation is valid when the absorption contribution is large in comparison with the scattering contribution. In practical terms this criterion is considered satisfied when the single scattering albedo[15,16] is less than 0.2. The albedo a is defined as

$$a = \frac{\sigma_s}{\sigma_e} \quad , \tag{B.1}$$

where σ_s is the scattering cross section per unit volume and σ_e is the extinction cross section per unit volume. Each bubble in the sediment will act as a scatterer with scattering cross section σ_s given by Eq. (3.9):

$$\sigma_S(r_b) = \frac{4\pi r_b^2}{\left[\left(\frac{f_r}{f}\right)^2 - 1\right]^2 + \delta^2} \quad . \tag{B.2}$$

The total bubble scattering cross section per unit volume σ_s is this expression integrated over the distribution of bubble radii:

$$\sigma_S = \int_0^\infty \sigma_S(r_b)\, f(r_b)\, dr_b \quad . \tag{B.3}$$

The extinction cross section σ_e associated with the same bubble is[17]

$$\sigma_e(r_b) = \frac{4\pi r_b^2 \left(\frac{\delta}{k_r r_b}\right)}{\left[\left(\frac{f_r}{f}\right)^2 - 1\right]^2 + \delta^2} \quad . \tag{B.4}$$

where K_r is the acoustic wavenumber at resonance,

$$k_r = \frac{2\pi f_r}{C} \quad . \tag{B.5}$$

The total extinction cross section per unit volume is the integral of Eq. (B.4) over the bubble size distribution.

$$\sigma_e = \int_0^{\infty} \sigma_e(r_b)\, f(r_b) dr_b \quad , \tag{B.6}$$

Upon inserting expressions (B.3) and (B.6) into expression (B.1) above, the single scattering albedo is given by

$$a = \frac{\int_0^{\infty} \sigma_s(r_b)\, f(r_b)\, dr_b}{\int_0^{\infty} \sigma_e(r_b)\, f(r_b)\, dr_b} \quad . \tag{B.7}$$

The integral in the numerator can be expressed as a sum of resonant and nonresonant contributions. The nonresonant part is negligible except in the case of very large bubbles. The remaining resonant contribution includes a delta function about the resonance radius. The value of this integral can therefore be approximated by simply evaluating the integrand at the resonance radius.

Computation of the albedo via expression (B.7) is nontrivial. In determining whether a single scatter model applies, however, it suffices simply to determine if the albedo is less than 0.2. The numerator can be estimated accurately by neglecting the nonresonant contribution as described above. If the denominator is approximated similarly, i.e., by evaluating its integrand at the resonance radius, any error incurred will make the denominator smaller. An approximate albedo, which can be defined as

$$\tilde{a} = \frac{\sigma_s(a_r)}{\sigma_e(a_r)} \quad , \tag{B.8}$$

will therefore be greater than or equal to the actual albedo given in expression (B.7). Therefore, if the approximate albedo $\tilde{a}$ is less than 0.2, a single scattering

model is sufficient. Upon combining Eq. (B.2), Eq. (B.4), and Eq. (B.8), $\tilde{a}$ becomes

$$\tilde{a} = \frac{k_r r_b}{\delta} \quad . \tag{B.9}$$

Medwin[18] showed that, for resonant bubbles, $f_r a_r$ is approximately 3 and δ is approximately 0.1. If these values are used, $\tilde{a}$ is evaluated at 0.126. A single scattering model is therefore appropriate.

This page intentionally left blank.

REFERENCES

1. F. A. Boyle and N. P. Chotiros, "Bottom Penetration at Shallow Grazing Angles II," Applied Research Laboratories Technical Report No. 92-12 (ARL-TR-92-12), Applied Research Laboratories, The University of Texas at Austin, June 1992.

2. M. Stern, A. Bedford, and H. R. Millwater, "Wave Reflection from a Sediment Layer with Depth-Dependent Properties," J. Acoust. Soc. Am. **77**(5), 1781-1788 (1985).

3. L. M. Brekhovskikh, *Waves in Layered Media* (Academic Press, New York, 1980).

4. E. K. Westwood, "Acoustic Propagation Modelling in Shallow Water using Ray Theory," Ph.D. Dissertation, The University of Texas at Austin, December 1988.

5. W. H. Beyer, ed., *CRC Standard Mathematical Tables, 25th edition* (CRC Press, Boca Raton, Florida, 1981).

6. Ibid., Boyle and Chotiros.

7. Ibid., Stern, Bedford, and Millwater.

8. J. A. Hawkins, "A Variational Model for Bubbly Sediments with a Distribution of Bubble Sizes," Ph.D. Dissertation, The University of Texas at Austin, May 1992.

9. S. D. Howkins, "Measurements of the Resonant Frequency of a Bubble near a Rigid Boundary," J. Acoust. Soc. Am. **37**, 504 (1965).

10. R. Wildt, ed., "Acoustic Theory of Bubbles," in *Physics of Sound in the Sea*, N.D.R.C. Summary Technical Report Div. 6, Washington, D.C. (1946), Chap. 28, Vol. 8.

11. M. Minneart, "On Musical Air-Bubbles and the Sounds of Running Water," Phil. Mag. **26**, 235 (1933).

12. H. Medwin, "Acoustical Determinations of Bubble Size Spectra," J. Acoust. Soc. Am. **62**(4), 1041-1044 (1977).

13. J. L. Finney and J. Wallace, J. Non-Cryst. Solids **34**, 165 (1981).

14. G. S. Cargill, "Radial Distribution Functions and Microgeometry of Dense Random Packings of Hard Spheres," *in Physics and Chemistry of Porous Media*, D. L. Johnson and P. N. Sen, editors (American Institute of Physics, New York, 1984).

15. D. R. Jackson, D. P. Winebrenner, and A. Ishimarv, "Application of the Composite Roughness Model to High-Frequency Bottom Backscattering," J. Acoust. Soc. Am **79**, 1410-1422 (1986).

16. F. T. Ulaby, R. K. Moore, and A. K. Fung, *Microwave Remote Sensing, Active and Passive* (Addison-Wesley, Reading, Massachusetts, 1982).

17. H. Medwin, "Counting Bubbles Acoustically, A Review," Ultrasonics, 7-13 (1977).

30 July 1993

DISTRIBUTION LIST FOR
ARL-TR-93-15
Final Report Under Contract N00039-91-C-0082,
TD No. 01A1029, Bottom Backscatter from Trapped Bubbles

Copy No.

Commanding Officer
Naval Research Laboratory
Stennis Space Center, MS 39529-5004

1	Attn:	R. Farwell (Code 7174)
2		D. Young (Code 7331
3		P. Fleischer (Code 7430)
4		K. Briggs (Code 7430)
5		P. Valent (Code 7401)
6		R. Love (Code 7174)
7		B. Adams (Code 7180)
8		E. Franchi (Code 7105)
9		S. Stanic (Code 7174)
10		D. Ramsdale (Code 7170)
11		M. Richardson (Code 7430)
12		R. Meredith (Code 7172)
13 - 24		Library (Code 7035.3)

Office of Naval Research
Department of the Navy
Arlington, VA 22217-5000

25	Attn:	J. Kravitz (Code 1125GG)
26		M. Badiey (Code 1125OA)
27		T. Simmen (Code 1125OA)
28		J. Beebe (Code 4433C)
29		E. Chaika (4431)
30		W. Ching (Code 4433)
31		T. Goldsberry (Code 4410)
32		D. Houser (Code 4424)

Commanding Officer
Naval Oceanographic Office
Stennis Space Center, MS 39522-5000

33	Attn:	J. Bunce (Code OW)
34		E. Beeson (Code OARR)

Distribution List for ARL-TR-93-15 under Contract N00039-91-C-0082, TD No. 01A1029
(cont'd)

Copy No.

Commander
Naval Oceanography Command
Stennis Space Center, MS 39522-5000
35 Attn: D. Durham (Code N5A)
36 R. L. Matin

Commander
Naval Sea Systems Command
Department of the Navy
Arlington, VA 22242-5160
37 Attn: J. Grembi (PMO407B)
38 D. Gaarde (PMO407-2)

G & C Systems Manager
MK48/ADCAP Program Office
National Center 2
2521 Jefferson Davis Hwy
12W32
Arlington, VA 22202
39 Attn: H. Grunin (PMO402E1)

Program Manager
MK50 Torpedo Program Office
Crystal Park 1
2011 Crystal Drive
Suite 1102
Arlington, VA 22202
40 Attn: T. Douglass (PMO406)

Commander
Dahlgren Division
Naval Surface Warfare Center
Dahlgren, VA 22448-5000
41 Attn: Library

Commander
Dahlgren Division
Naval Surface Warfare Center
Silver Spring, MD 20903-5000
42 Attn: S. Martin (Code U24)
43 J. Sherman (Code U20)
44 M. Stripling (Code U04)

Distribution List for ARL-TR-93-15 under Contract N00039-91-C-0082, TD No. 01A1029
(cont'd)

Copy No.

Commanding Officer
Coastal Systems Station, Dahlgren Division
Naval Surface Warfare Center
Panama City, FL 32407-5000

45 Attn: M. Hauser
46 R. Johnson (Code 210T)
47 R. Lim
48 E. Linsenmeyer
49 D. Todoroff (Code 2120)

Commander
Naval Undersea Warfare Center Division
New London, CT 06320-5594

50 Attn: W. Roderick (Code 33A3)
51 J. Chester (Code 3331)
52 P. Koenig (Code 3331)

Advanced Research Projects Agency
3701 North Fairfax Drive
Arlington, VA 22203-1714

53 Attn: W. Carey

Commander
Naval Undersea Warfare Center Division
Newport, RI 02841-5047

54 Attn: J. Kelly (Code 3632)
55 F. Aidala (Code 362)
56 W. Gozdz (Code 36291)

Officer in Charge
Arctic Submarine Lab Detachment
Naval Undersea Warfare Center
49250 Fleming Rd.
San Diego, CA 92152-7210

57 Attn: R. Anderson (Code 19)

Distribution List for ARL-TR-93-15 under Contract N00039-91-C-0082, TD No. 01A1029
(cont'd)

Copy No.		
	Chief of Naval Operations Department of the Navy Washington, DC 20360	
58	Attn:	R. Widmayer (OP 374T)
59		R. Winokur (OP 096T)
60		K. Martello (OP 954F1)
61		T. Fraim (OP 986G)
62		R. James (OP 006DX)
63		H. Montgomery (OP 9878)
64		J. Boosman (OP 987J)
	Commander Mine Warfare Command Charleston Naval Base Charleston, SC 29408	
65	Attn:	G. Pollitt (Code N3A)
66		B. O'Connel (Code N3A)
	Commanding Officer and Director Defense Technical Information Center Cameron Station, Building 5 5010 Duke Street	
67 - 78	Alexandria, VA 22314	
	Applied Physics Laboratory The University of Washington 1013 NE 40th Street Seattle, WA 98105	
79	Attn:	D. Jackson
80		Library
	Applied Research Laboratory The Pennsylvania State University P. O. Box 30 State College, PA 16804	
81	Attn:	R. Goodman
82		E. Liszka
83		Library
84		D. McCammon
85		S. McDaniel
86		F. Symons

Distribution List for ARL-TR-93-15 under Contract N00039-91-C-0082, TD No. 01A1029
(cont'd)

Copy No.	
	Presearch, Inc. 8500 Executive Park Avenue Fairfax, VA 22031
87 - 90	Attn: J. R. Blouin
	Physics Department The University of Texas at Austin Austin, TX 78712
91	Attn: W. D. McCormick
92	M. Fink
93	T. Griffy
	Aerospace Engineering Department The University of Texas at Austin Austin, TX 78712
94	Attn: M. Bedford
95	M. Stern
96	Robert A. Altenburg, ARL:UT
97	Hollis Boehme, ARL:UT
98	Frank Boyle, ARL:UT
99	Nicholas P. Chotiros, ARL:UT
100	John M. Huckabay, ARL:UT
101	Thomas G. Muir, ARL:UT
102	Library, ARL:UT
103 - 109	Reserve, ARL:UT